Research Paper https://doi.org/10.7733/jnfcwt.2017.15.2.125

The Corrosion Properties of Zr-Cr-NM Alloy Metallic Waste Form for Long-term Disposal

Zr-Cr-NM 금속폐기물고화체 합금의 장기처분을 위한 부식특성

Seungyoub Han*, Seon Ah Jang, Hee-Chul Eun, Jung-Hoon Choi, Ki Rak Lee, Hwan Seo Park, and Do-Hee Ahn
Korea Atomic Energy Research Institute, 111, Daedeok-daero 989beon-gil, Yuseong-gu, Daejeon, Republic of Korea

한승엽*, 장선아, 은희철, 최정훈, 이기락, 박환서, 안도희
한국원자력연구원, 대전광역시 유성구 대덕대로 989번길 111

(Received February 6, 2017 / Revised April 27, 2017 / Approved May 17, 2017)

KAERI is conducting research on spent cladding hulls and additive metals to generate a solidification host matrix for the noble metal fission product waste in anode sludge from the electro-refining process to minimize the volume of waste that needs to be disposed of. In this study, alloy compositions Zr-17Cr, Zr-22Cr, and Zr-27Cr were prepared with or without eight noble metals representing fuel waste using induction melting. The microstructures of the resulting alloys were characterized and electrochemical corrosion tests were conducted to evaluate their corrosion characteristics. All the compositions had better corrosion characteristics than other Zr-based alloys that were evaluated for comparison. Analysis of the leach solution after the corrosion test of the Zr-22Cr-8NM specimen indicated that the noble metals were not leached during corrosion under 500 mV imposed voltage, which simulates a highly oxidizing disposal environment. The results of this study confirm that Zr-Cr based compositions will likely serve as chemically stable waste forms.

Keywords: Pyrochemical process, Spent fuel cladding hull, Noble metal, Metallic waste form, Corrosion property

*Corresponding Author.
Seungyoub Han, Korea Atomic Energy Research Institute, E-mail: hsy@kaeri.re.kr, Tel: +82-42-866-6141

ORCID

Seungyoub Han	http://orcid.org/0000-0002-4290-8266	Seon Ah Jang	http://orcid.org/0000-0001-8354-3518
Hee-Chul Eun	http://orcid.org/0000-0001-8350-2935	Jung-Hoon Choi	http://orcid.org/0000-0003-0705-6771
Ki Rak Lee	http://orcid.org/0000-0001-9958-7742	Hwan Seo Park	http://orcid.org/0000-0002-0048-2690
Do-Hee Ahn	http://orcid.org/0000-0002-2661-9413		

KAERI에서는 파이로프로세싱에서 발생하는 금속폐기물의 부피 및 무게 감량을 위해 고방사성 장반감기 핵종을 포함하는 anode sludge내 NM의 고화매질로써 폐피복관과 첨가금속을 재활용하는 연구를 진행하고 있다. 본 연구에서는 Cr 함량을 조절한 Zr-17Cr-8NM, Zr-22Cr-8NM, Zr-27Cr-8NM 합금을 유도용융을 통해 제조하였고, 전기화학적 부식시험을 실시하여 부식특성을 평가하였다. 모든 조성에서 기존 연구 중인 Zr계 합금고화체 조성보다 우수한 부식특성을 나타냈다. 또한 Zr-22Cr-8NM 시편의 부식시험 후 침출용액 조성 분석 결과, 500 mV 전압 조건 이하에서는 NM 침출이 없었고 이를 통해 우수한 화학적 안정성을 갖는 합금고화체 조성을 확보하였다.

중심단어: 파이로 프로세싱, 폐피복관, 귀금속, 금속폐기물고화체, 부식특성

1. Introduction

Research, mainly published in the United States, has studied the technologies used in solidification processing by melting spent nuclear fuel assembly materials and hulls for metal waste reduction that occurs during the pyro-processing [1-7]. Cladding hulls in spent fuel assemblies from a domestic PWR are composed of a metal alloy such as Zircaloy-4, Zirlo, stainless steel, or Inconel and account for the highest volume and weight fraction in pyro-processing wastes [8-10]. In particular, the contaminated cladding hulls are classified as low- and intermediate-level waste in the Korean domestic standard, but they are classified as GTCC waste in the US standard owing to residual nuclear fuel, fission product permeation, and activation of the cladding hull materials [1]. In other words, decontamination is essential to the development of volume reduction and recycling technology for cladding hulls and for a significant proportion of the waste generated by pyro-processing to be classified as low- or intermediate-level waste. Currently, France has been operating a commercial facility where high-pressure compaction processes are used for volume reduction of the cladding hulls after wet reprocessing. In the United States, a demonstration facility for melting and solidifying stainless steel cladding hulls after pyro-processing has been recently developed and operated [11]. Recently, at KAERI, we have been conducting research on using Zirlo cladding hulls as a host matrix to solidify and handle highly radioactive anode sludge residue that includes noble metal (NM) fission products from electro-refining in pyro-processing. If we produce a Metallic Waste Form (MWF) by adding alloying elements and anode sludge to the cladding hulls, the overall waste volume can be minimized because the cladding hulls can be used as the solidification host matrix for fuel wastes in the MWF. Although stable waste forms can be made with the SS-15Zr alloy developed for steel cladding, this is disadvantageous for domestic cladding hull disposal efficiency because the Zr content is low [2-6]. In addition, the mechanical stability and corrosion resistance of the Zr-8SS alloy is relatively low [12]. As a result of the new composition with Zr-Cr in KAERI, a stable MWF was formed without cracks. The chemical durabilities of representative Zr-Cr alloys are being evaluated as possible waste forms for the cladding hull and anode sludges generated from the pyro-processing.

2. Experimental Procedures

The chemical compositions of the Zr-Cr based alloys used in this study are shown in Table 1. The Zr-22Cr composition has a eutectic point composition and the Zr-27Cr and Zr-17Cr compositions vary the Cr concentration by ±5 wt%, respectively. Three additional alloys were prepared by adding 8 wt% total NM to each of the three Zr-Cr based MWF alloy compositions. For convenience of descrip-

Table 1. Chemical compositions of specimens (wt%)

Element		ZC (Host Matrix Alloy)			ZCN (Metal Waste Form Alloy)		
		Z17C	Z22C	Z27C	Z17C8N	Z22C8N	Z27C8N
Zr		Bal.	Bal.	Bal.	Bal.	Bal.	Bal.
Cr		17	22	27	15.6	20.2	24.8
NM	Mo	-	-	-	2	2	2
	Ru	-	-	-	2	2	2
	Pd	-	-	-	2	2	2
	Re	-	-	-	2	2	2

tion, the materials are referred to as Z17C, Z22C, Z27C, Z17C8N, Z22C8N, and Z27C8N according to the composition. All the specimens were fabricated by high frequency induction heating in a silica crucible in an Ar atmosphere after a vacuum of 5×10^{-5} torr was formed. To ensure the uniformity of the specimen, it was held at 1650 to 1750°C for 5 minutes. After the melt was completely formed, it was kept at 1350°C for about 15 minutes, furnace cooling was then applied to reduce the solidification shrinkage cracks and porosity. All the prepared specimens were cut and polished, and XRD, SEM, and EDS analyses were performed for a microstructure and phase analysis. To evaluate the corrosion properties, potentiodynamic (PD) and potentiostatic (PS) tests were carried out in an acidic brine aqueous solution (0.0001 mol·kg^{-1} H_2SO_4 + 0.01 mol·kg^{-1} NaCl in demineralized water, adjusted to pH 4) [7]. The solutions from the PS tests were analyzed using ICP-MS.

3. Results and Discussion

To relate the corrosion properties to the microstructure, the phases and microstructure of the six Zr-Cr-based metal alloys were analyzed. As a result of the XRD analyses, which are shown in Fig. 1, the main phases of all the specimens were α-Zr, $ZrCr_2$, and Zr_2Si, and the secondary phases were $CrSi_2$, Zr_3Si_2, ZrSi, and Cr and Si single phases. This indicates that the Si from the crucible surface reacted with the melt. The NM elements were mostly dissolved in the main phases. Fig. 2 shows the microstructure of the Z22C specimen by SEM image and EDS mapping, and the results of EDS composition analysis of each phase are shown in Table 2. In the SEM observation, the α-Zr phase of the first region is white, the Zr_2Si phase of the second region is gray, and the $ZrCr_2$ phase of the third region is black. The α-Zr, Zr_2Si, and $ZrCr_2$ phases coexist as the eutectic structure of the fourth region (Fig. 2(b)). Fig. 3 shows the microstructures of the Z17C, Z22C, and Z27C specimens with a solidification host matrix composition observed using SEM, and the fraction of each phase in the microstructures is shown in Table 3. As shown in Fig. 3, the Z22C specimen has a large eutectic structure (yellow arrows) with a unit size of about 30 μm. The Z17C and Z27C specimens have a high fraction of α-Zr (white arrow), and a $ZrCr_2$ (black arrows) phase was formed with a coarse size of over 50 μm. Zr_2Si phases (gray arrows) with various sizes (5 to 20 μm) and shapes were formed in the α-Zr region in all the specimens. Based on the volume fraction analysis shown in Table 3, the Z22C specimen made with the eutectic composition showed the highest eutectic structure fraction of 45 vol%, and the Z17C specimen had the highest fraction of α-Zr owing to the high Zr weight fraction. The Z27C specimen exhibited a relatively high volume fraction with eutectic structure and the highest $ZrCr_2$ phase volume fraction owing to the high Cr

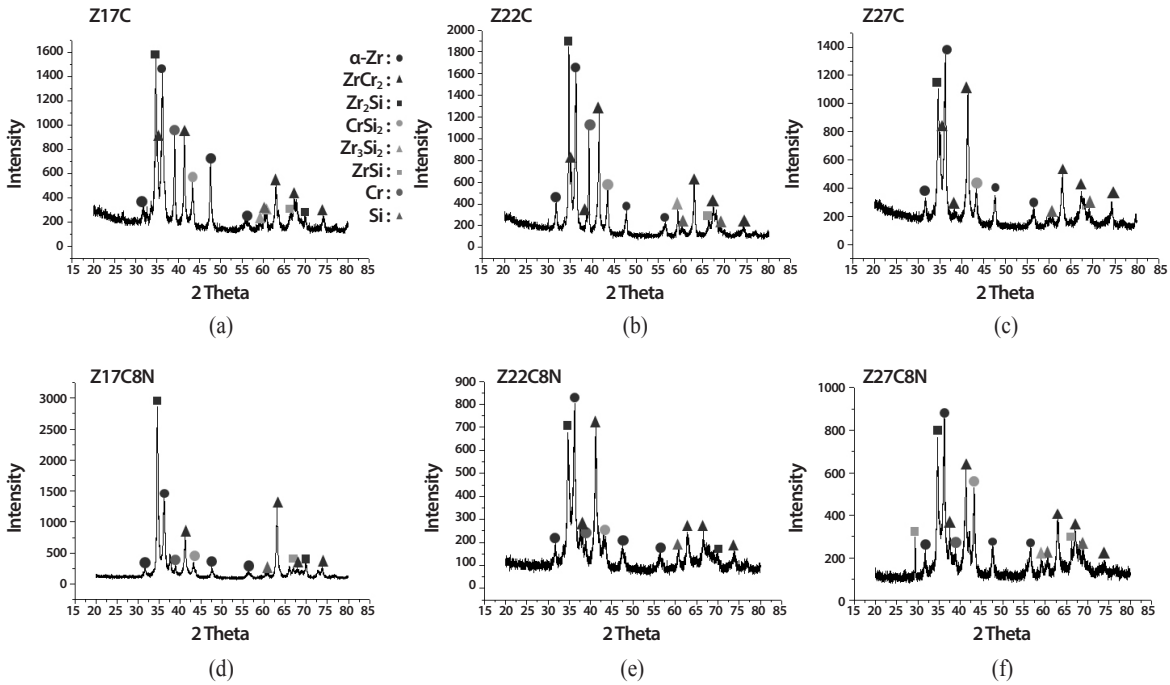

Fig. 1. X-ray diffraction results of the (a) Z17C, (b) Z22C, (c) Z27C, (d) Z17C8N, (e) Z22C8N, and (f) Z27C8N specimens.

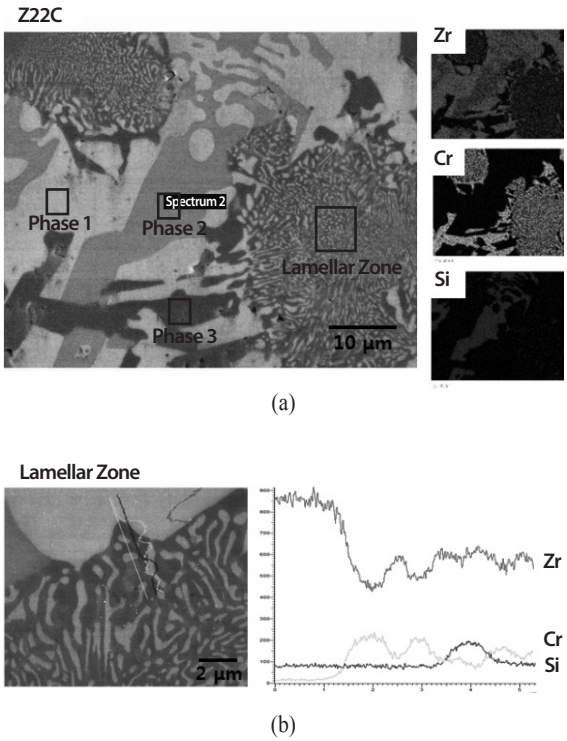

Fig. 2. EDS mapping results of the (a) Z22C specimen and (b) lamellar zone.

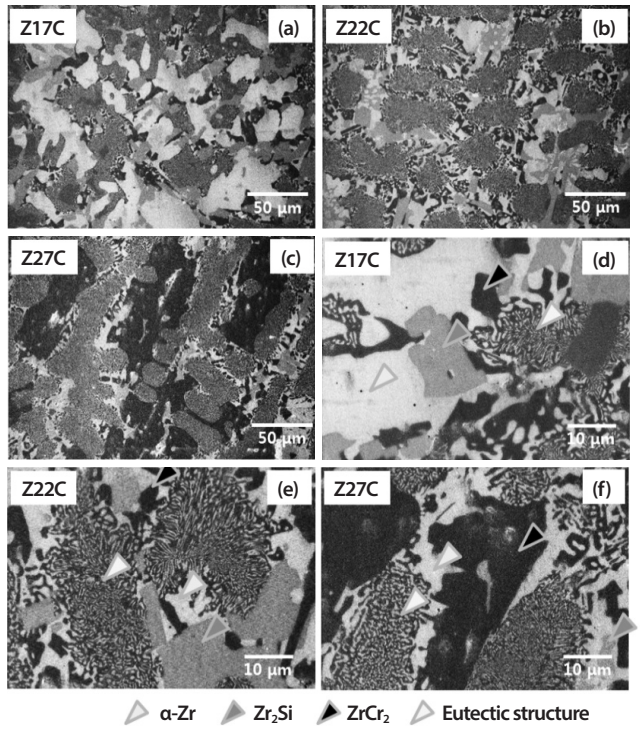

Fig. 3. SEM micrographs of the (a) and (d) Z17C, (b) and (e) Z22C, (c) and (f) Z27C specimens.

Table 2. EDS analysis results of the Z22C specimens (at.%)

Element	Phase 1 (α-Zr)	Phase 2 (Zr_2Si)	Phase 3 ($ZrCr_2$)	Lamellar Zone
Zr	100.0	68.0	38.9	53.7
Cr	-	-	61.1	40.8
Si	-	32.0	-	5.5

Table 3. Phase volume fractions of the ZC specimens (vol.%)

Phase	Z17C	Z22C	Z27C
α-Zr	55	25	20
$ZrCr_2$	15	15	35
Zr_2Si	10	15	10
Eutectic structure	20	45	35

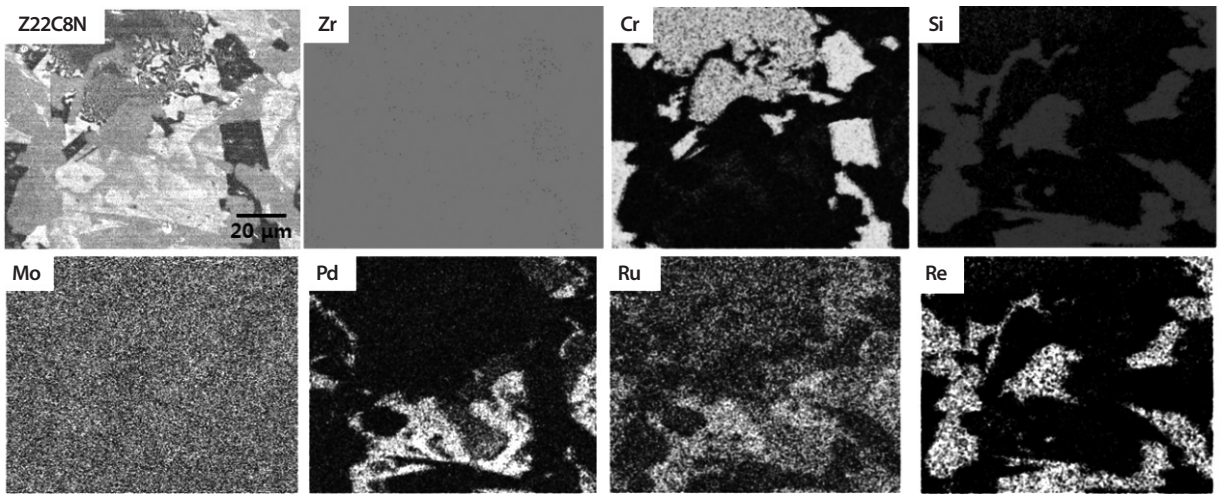

Fig. 4. EDS mapping results of the Z22C8N specimen.

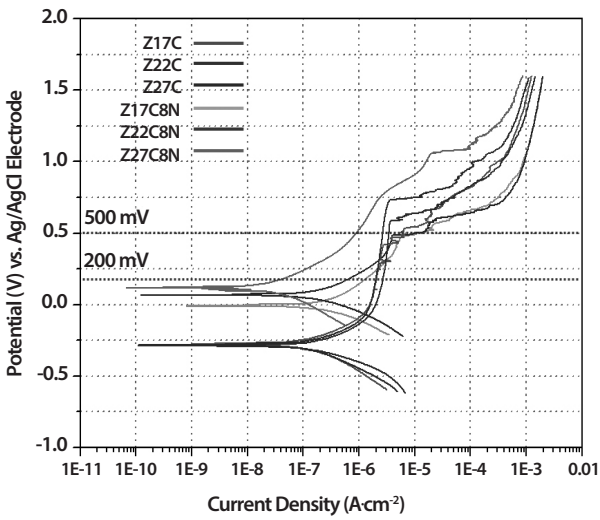

Fig. 5. The potentiodynamic polarization plots for ZC and ZCN specimens test at acidic brine solution.

weight fraction.

Fig. 4 shows the EDS mapping results for the Z22C8N specimen. The Zr is uniformly distributed in the whole area, and Cr and Si form intermetallics with Zr. The NM elements were distributed differently: Mo was uniformly distributed in the whole area, Pd and Ru were concentrated in α-Zr, Ru was partially detected in the $ZrCr_2$ phase, and Re, which is a surrogate for Tc, was mostly concentrated in Zr_2Si.

PD and PS tests were carried out to evaluate the corrosion properties of the specimens and the microstructures were observed before and after the test to identify active phases. Fig. 5 shows the I-V curves obtained from the PD tests with each specimen. The voltage range was set to -0.5 to 1.5 V. The E_{corr} and I_{corr} values were determined by

Table 4. Key parameters from polarization plot for the various Zr and NM alloys [13]

Alloy	E_{corr} (mV)	I_{meas} ($A \cdot cm^{-2}$)		
		at E_{corr}	at 200 mV	at 500 mV
Z17C	-271	1.83×10^{-7}	2.10×10^{-6}	6.01×10^{-6}
Z22C	-280	1.30×10^{-7}	2.05×10^{-6}	2.65×10^{-6}
Z27C	-293	1.16×10^{-7}	2.76×10^{-6}	3.41×10^{-6}
Z17C8N	-17	2.98×10^{-7}	1.51×10^{-6}	1.18×10^{-5}
Z22C8N	6	2.05×10^{-7}	8.13×10^{-7}	1.08×10^{-5}
Z27C8N	128	2.55×10^{-8}	5.87×10^{-8}	8.88×10^{-7}
Zr	≒ -409	1.6×10^{-8}	3.0×10^{-7}	6.2×10^{-3}
Zircaloy-4	≒ -170	2.5×10^{-7}	1.5×10^{-5}	2.0×10^{-3}
Zr-8SS-2NM	≒ -45	4.1×10^{-8}	3.6×10^{-6}	3.9×10^{-2}
EWF	≒ 35	9.5×10^{-8}	1.8×10^{-6}	4.5×10^{-6}

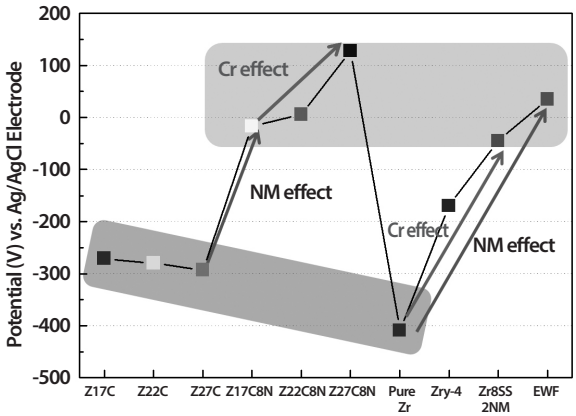

Fig. 6. Comparison of corrosion potential values for the various alloys [13].

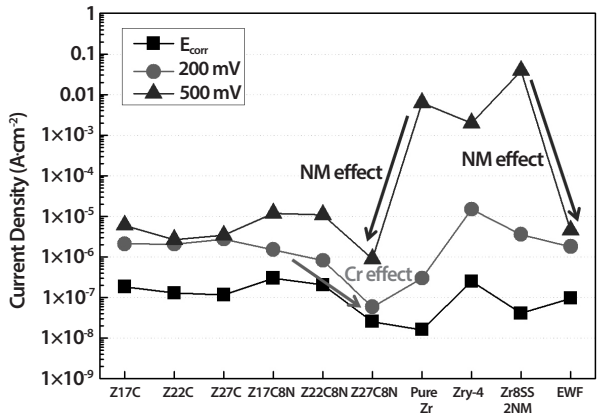

Fig. 7. Comparison of corrosion current density values for the various alloys [13].

Tafel extrapolation from the curves of each specimen, and the currents (I_{meas}) were measured at 200 mV and 500 mV. Table 4 shows the results of these corrosion tests and results of the tests performed with other alloys using the same test conditions in this study, including pure Zr, Zircaloy-4, Zr-8SS-2NM, and a NM-only alloy (EWF: Epsilon-metal Waste Form), respectively [7,13,14]. Fig. 6 shows a graph comparing E_{corr} values measured in the PD tests. In the Zr-Cr alloys, the E_{corr} value increased about 300 to 400 mV due to the addition of NM. The same tendency of E_{corr} to increase as the NM composition increased has been observed in other research results [13,14]. The Z17C8N-27C8N alloy had a higher Ecorr than Zr-8SS-2NM and the Z27C8N alloy had a higher E_{corr} than EWF. Fig. 7 shows a graph comparing current values measured at E_{corr}, 200 mV, and 500 mV in the PD test. The I_{corr} values at E_{corr} are similar

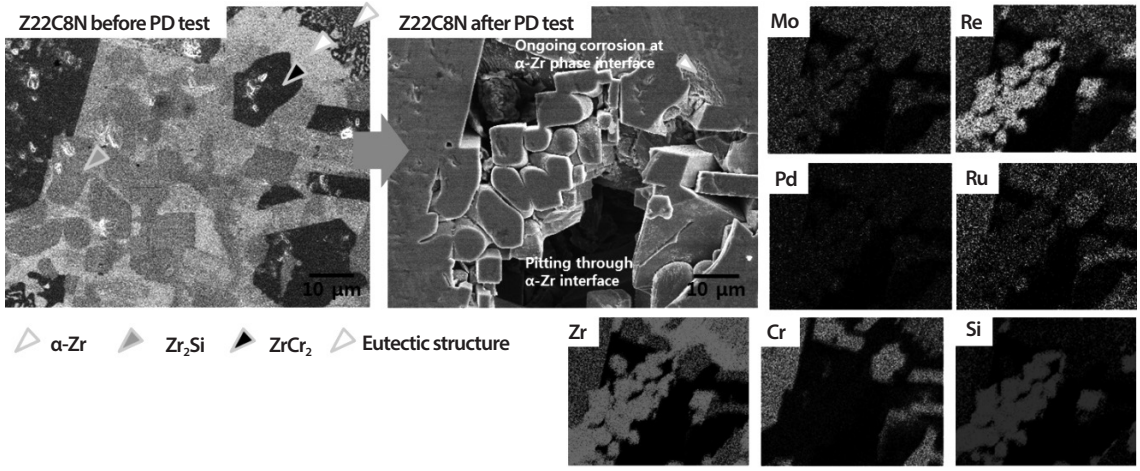

Fig. 8. SEM micrographs of the Z22C8N specimen before and after potentiodynamic test, and EDS mapping results of the Z22C8N specimen after potentiodynamic test.

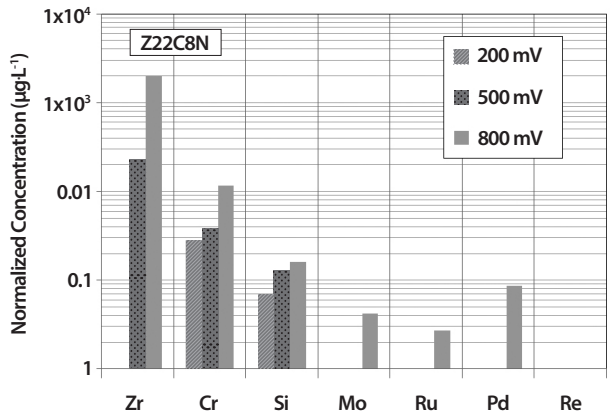

Fig. 9. ICP analysis results of electrolyte after potentiostatic test at 200 mV, 500 mV, and 800 mV potential conditions.

for all the specimens including the comparative materials, but relatively large differences are seen at 200 mV and 500 mV. Pure Zr, Zircaloy-4, and Zr-8SS-2NM materials have I_{meas} values of about 0.01 $A \cdot cm^{-2}$ at 500 mV, which are about 1000 times higher than currents measured for the Zr-Cr alloy and NM alloy. The Zr-Cr-NM alloy specimen had a higher E_{corr} value and a lower I_{corr} value than the Zircaloy-4 cladding material or the Zr-SS-NM MWF alloy. This means that, under these conditions, the Zr-Cr-NM alloys have lower corrosion rates than other Zr-based alloys.

Fig. 8 shows the microstructure and element distribution of the Zr-22Cr-8NM specimen in the same area before and after the PD test. When the applied voltage was increased to 1.5 V, the α-Zr region containing Mo, Pd, and Ru was largely corroded, but the $ZrCr_2$ phase containing Mo and Ru and the Zr_2Si phase containing Mo and Re mostly remained. Most of the corrosion was concentrated at the phase interfaces, but corrosion rarely occurred in the eutectic structure, which had a large amount of phase interfaces between various phases.

The PS tests were carried out at 200 mV, 500 mV, and 800 mV for 3 hours in the same electrolyte solution composition, volume and working electrode surface area as the PD test, and the analysis results of the composition of the leachate are shown in Fig 9. In the case of NM elements, leaching occurred only at 800 mV, while leaching of elements forming the host matrix tended to increase with an increase in voltage. Most of the Pd was leached from α-Zr, which was highly corrosive, and the amount of Ru leached mostly from $ZrCr_2$ was small, while Mo was leached at a medium level. In particular, the Re enriched in Zr_2Si did not leach under any voltage conditions. The Zr_2Si phase showed high corrosion resistance and effectively immobilized Re despite the absence of Cr, which contributed highly

to the improvement in corrosion resistance of other phases. The Zr_2Si phase formed from Si released from the crucible during alloy production is a very stable phase. The addition of Si as a trim chemical should be investigated.

4. Conclusion

In this study, we evaluated the use of spent cladding hulls and added Cr as a solidification host matrix for NM waste in the anode sludge generated in the electro-refining process. Three Zr-Cr alloys simulating the solidification host matrix and three Zr-Cr-NM alloys simulating the final metal waste form alloy were prepared using an induction melting method. The microstructure and corrosion characteristics of the different Zr-Cr alloys were compared and analyzed. The main phases composing the Zr-Cr alloy consisted of α-Zr, $ZrCr_2$, and Zr_2Si. The eutectic structure and $ZrCr_2$ phase increased with an increasing Cr content. Pd was concentrated in α-Zr; Ru in α-Zr and $ZrCr_2$; Re in Zr_2Si; and Re in the Zr_2Si phase. Electrochemical corrosion tests were carried out on the Zr-Cr and Zr-Cr-NM alloys prepared in this study, and the results of the PD tests were compared with results for other Zr-based alloys. The Zr-Cr-NM alloys exhibited high corrosion resistances and low corrosion rates compared to conventional materials. As a result of the analysis of the composition of the leachate after the PS test, the NM elements were not leached in tests conducted at potentials under 500 mV, and Re, which is a surrogate Tc, was not leached in the test at 800 mV. In particular, the Zr_2Si phase, which is the encapsulating phase of Re, was very stable and showed no shape change or leaching of Re after the corrosion tests, suggesting that the immobilization of Tc will be excellent. Through this study, we concluded that it is likely that Zr-Cr alloys will be effective waste forms for spent cladding hulls generated by pyro-processing. The corrosion properties appear to be suitable for long-term disposal of high radioactive metallic waste.

ACKNOWLEDGMENTS

This work was supported by the National Research Foundation of Korea (NRF) grant funded by the Korea government (MSIP) (No. 2012M2A8A5025801).

REFERENCES

[1] Brian R. Westphal, S. M. Frank, W. M. McCartin, D. G. Cummings, J. J. Giglio, T. P. O'Holleran, P. A. Hahn, T. S. Yoo, K. C. Marsden, K. J. Bateman, and M. N. Patterson, "Characterization of Irradiated Metal Waste from the Pyrometallurgical Treatment of Used EBR-II Fuel", Metall. Mater. Trans. A, 46(1), 83-92 (2015).

[2] Daniel P. Abraham, Sean M. McDeavitt, and Jangyul Park, "Microstructure and Phase Identification in Type 304 Stainless Steel-Zirconium Alloys", Metall. Mater. Trans. A, 27(8), 2151-2159 (1996).

[3] S. M. Frank, D. D. Keiser Jr, and K. C. Marsden, Immobilization of Technetium in a Metallic Waste Form, Global 2007, INL/CON-07-12883 (2007).

[4] D. D. Keiser Jr, D. P. Abraham, W. Singkler, J.W. Richardson Jr, and S.M. McDeavitt, "Actinide distribution in a stainless steel-15wt% zirconium high-level nuclear waste form", J. Nucl. Mater, 279(2-3), 234-244 (2000).

[5] D. D. Keiser Jr, D. P. Abraham, and J.W. Richardson Jr, "Influence of technetium on the microstructure of a stainless steel-zirconium alloy", J. Nucl. Mater, 277(2-3), 333-338 (2000).

[6] S. M. McDeavitt, D. P. Abraham, and J. Y. Park, "Evalution of stainless steel-zirconium alloys as high-level nuclear waste forms", J. Nucl. Mater, 257(1), 21-34 (1998).

[7] W. L. Ebert and D. Kolman, Alloy Waste Form Testing Strategy Roadmap, U.S. Department of Energy Report, FCRD-SWF-2013-000226 (2013).

[8] P. S. Song, W. K. Choi, B. Y. Min, H. I. Kim, C. H. Jung, and W. Z. Oh, "Melting Treatment Technology of Radioactive Metal Waste and Characteristics of the Radio-

nuclide Distribution", JNFCWT, 22(3), 213-225 (2005).
[9] M.K. Jeon, C.H. Lee, C.J. Park, K.H. Kang, and G.I. Park, Effect of burn-up on the radioactivation behavior of cladding materials, Korea Atomic Energy Research Institute Technical Report, KAERI/TR-5100 (2013).
[10] JB Wattecamps, N. Hubert, and T. Zanife, "Legacy Waste Retrieval from Cladding Hulls and Fuel Hardware Storage", WM Conf., Tucson (2007).
[11] Thierry Advocat, Catherine Andrieux, Isabelle Bardez, Florence Bart, Pascal Bouniol et al., Nuclear Waste Conditioning, A Nuclear Energy Division Monograph (2009).
[12] N. Das, G. Abraham, P. Sengupta, Ashok Arya, V. Kain, and G. K. Dey, "Microstructural analysis and corrosion behavior of zirconium-stainless steel metallic waste form", J. Nucl. Mater, 467(2), 489-499 (2015).
[13] W. L. Ebert, T.A. Cruse, J.E. Indacochea, and V.K. Gattu, Corrosion Tests with Alloyed Waste Forms Made with Type 316L Stainless Steel, U.S. Department of Energy Report, FCRD-MRWFD-2015-000146 (2015).
[14] W. L. Ebert, Radionuclide Source Term Model for Metallic Waste Forms, U.S. Department of Energy Report, FCRD-SWF-2014-000244 (2014).